Int J Adv Manuf Technol (2016) 83:55–65
DOI 10.1007/s00170-015-7539-7

ORIGINAL ARTICLE

Chip formation and its effects on cutting force, tool temperature, tool stress, and cutting edge wear in high- and ultra-high-speed milling

Xiaobin Cui[1] · **Bo Zhao**[1] · **Feng Jiao**[1] · **Jianxin Zheng**[1]

Received: 7 April 2015 / Accepted: 2 July 2015 / Published online: 19 July 2015

Abstract In the present study, experimental tests and finite element simulation were conducted in order to investigate chip formation and its effects on cutting force, tool temperature, tool stress, and cutting edge wear in high- and ultra-high-speed (v=200~2000 m/min) milling. It was found that the serration of chip became more and more obvious as the cutting speed increased. Most of the saw-tooth chip was separated at the cutting speed of 2000 m/min. During the formation process of the separated saw-tooth, the high temperature in the shear band had substantial effect on the initiation of the crack in the chip. When the cutting speed increased, the formation frequency of the saw-tooth increased with decreasing growth rate and the tool-chip contact length exhibited a decreasing trend. At each cutting speed used in the present work, the fluctuation frequency of cutting force, tool temperature, and tool stress was consistent with that of the saw-tooth formation. The saw-tooth formation which led to periodically changing cutting thickness had great effects on the cyclical fluctuations of the cutting force, tool temperature, and tool stress. When the cutting speed increased from 650 to 2000 m/min, the amplitude of the cutting force and tool temperature grew 116 and 93 %, respectively. The higher degree of chip serration at higher cutting speed resulted in the substantial change of the cutting thickness, leading to greater mechanical and thermal impact. The tool temperature had greater effect on the tool stress than the cutting force did when the cutting speed was relatively high. Due to the small tool-chip contact length at cutting speeds of 1550 and 2000 m/min, no obvious wear appeared on the tool rake face. Because of the higher average value and the higher amplitude of tool stress at the cutting speed of 2000 m/min, chipping emerged on the tool cutting edge. This phenomenon was not found on the cutting edge when the cutting speed was 1550 m/min.

Keywords Chip formation · Cutting force · Tool temperature · Tool stress · Tool wear · High-speed milling

1 Introduction

The cutting tool and the workpiece interact with each other in the cutting process. On the one hand, some part of the workpiece is removed in the form of chip. On the other hand, due to the combined effects of mechanical and thermal loads, the cutting tool starts to wear until the failure criterion is reached. The chip morphology and chip formation mechanisms reflect the characteristics of the mechanical and thermal loads, which subsequently have great effects on the tool failure mechanisms [1–3]. Wang et al. [1] investigated the chip formation process and the variation of chip morphology in high-speed milling of hardened steel. They also studied the formation condition of continuous and saw-tooth chips and various characteristics of the saw-tooth chip. Ultra-high-speed milling tests of AerMet100 using nano TiAlN-coated carbide tools were performed by Su and Liu [2]. It was found that the tool wear mechanism was greatly influenced by the cutting temperature and workpiece mechanical properties. High-speed face milling of AISI H13 hardened steel was conducted by Cui and Zhao [3]. The characteristics of chip morphology, tool life, tool wear mechanisms, and surface roughness were analyzed for different cutting conditions.

It has been more than 80 years since Salomon [4] proposed the concept of high-speed cutting (HSC). Due to its

✉ Xiaobin Cui
kokcxb@163.com

[1] School of Mechanical and Power Engineering, Henan Polytechnic University, Jiaozuo 454003, People's Republic of China

advantages such as higher machining efficiency, lower cutting force, and better surface finish, HSC technology has been widely used in the manufacturing of automotive components and aluminum aeronautical. With the development of the cutting tool material and machine tools, increasingly high cutting speed has been used by the industries in order to stay competitive [5]. When relatively high cutting speed is applied, continuous saw-tooth chip arise in the metal cutting process. Chip with unusual morphology including sphere-like chip [3, 5, 6] and separated saw-tooth chip [3, 6, 7] will appear when the cutting speed is further increased. The emergence of separated saw-tooth chip is considered by some investigators [7] as the unique characteristics in ultra-high-speed cutting.

Theories for the saw-tooth chip formation mechanisms can be classified into two kinds, namely the adiabatic shear theory [8, 9] and the cyclic crack theory [10, 11]. Previous researches on chip formation mechanisms mainly focused on the explanation of the continuous saw-tooth chip. Relatively few studies [7, 12] were conducted to investigate the formation of separated saw-tooth chip. High-speed orthogonal cutting of Inconel 718 alloy was conducted by Su [7] to identify the chip formation mechanisms in different cutting speed ranges. The analysis results showed that the formation of separated saw-tooth chip can be explained by the cyclic crack theory. Finite element simulation was used by Guo and Yen [12] to investigate the formation mechanisms of discontinuous chip (separated saw-tooth chip) which arose in the cutting of AISI 4340 steel. It was found that adiabatic shearing contributed greatly to the formation of the discontinuous chip. Since the chip stem from the interaction between the cutting tool and the workpiece, there exist strong correlations between the chip formation and the loads which are exerted on the cutting tools. However, scant research was conducted to investigate the effects of chip morphology and chip formation mechanisms on mechanical and thermal loads in high- and especially ultra-high-speed cutting. Finite element simulation of cutting of AISI 4340 steel was conducted by Guo and Yen [12], and relationship between the fluctuation of cutting forces and the characteristics of chip formation was analyzed. The analysis results showed that compared with the cutting force in the formation process of the usual serrated chip, the cyclical fluctuation of the cutting force was intenser when the separated saw-tooth chip arose. Moreover, it was found that the force pattern was in-phase with the separated saw-tooth chip shape.

It can be found that much valuable information on chip morphology and chip formation in high-speed cutting has been provided by the previous studies. However, relatively few researches were conducted to investigate the formation mechanisms of the separated saw-tooth chip and there still existed controversy. It should be noted that scant research was performed to investigate the effects of separated saw-tooth formation on the mechanical and thermal loads in the cutting process. Moreover, thorough understanding of the mechanical and thermal loads in ultra-high-speed cutting (characterized by the separated saw-tooth chip) was very important for the analysis of tool failure mechanisms. Thus, it is critical to identify the characteristics of chip formation and its effects on cutting force, tool temperature, tool stress, and tool wear in ultra-high-speed cutting.

AISI H13 tool steel has been widely applied in hot forging, extrusion, and pressure die casting because of the advantages such as large high-temperature strength and great wear resistance [13, 14]. Therefore, in the present study, experimental tests and finite element simulation of high- and ultra-high-speed milling of AISI H13 hardened steel are conducted. Chip morphology and chip formation mechanisms at different cutting speeds (especially at ultra-high cutting speed) are analyzed and compared. Time domain and frequency domain characteristics of the cutting force, tool temperature, and tool stress obtained at different cutting speeds were identified and compared. Influences of chip formation on cutting force, tool temperature, tool stress and wear of the tool cutting edge are studied.

2 Experimental procedures and finite element simulation

2.1 Workpiece and cutting tool

In the present study, a block of AISI H13 hardened steel which was hardened to 46~47 HRC was used in the milling experiments. Chemical composition of the hardened steel under consideration is shown in Table 1. Tool holder with a diameter of 80 mm was applied. Only one of the teeth was used in the milling tests. Therefore, the effects of the tool tip run out on tool wear can be eliminated [15]. Tungsten carbide inserts were utilized. The insert contained 94 wt.% WC and 6 wt.% Co. Details of the tool geometry are shown in Fig. 1. The corner radius of the cutting tool was manufactured to be 0.1 mm. All the tests were carried out on a vertical computer numerically controlled machining center DAEWOO ACE-V500. The machining center with a 15-kW drive motor had a maximum spindle rotation speed of 10,000 rpm. The positioning accuracy and repetitive positioning accuracy of the machining center were ±5 and ±2 μm, respectively.

2.2 Cutting tests

Symmetric milling was applied for all the milling tests. Cutting speeds v (200, 650, 1100, 1550, and 2000 m/min) in the range of 200 to 2000 m/min were used. Radial depth of cut a_e, axial depth of cut a_p, and feed per tooth f_z were fixed to be 6, 0.4, and 0.04 mm/tooth, respectively. Relatively small values of radial depth of cut and feed per tooth were adopted

Table 1 Chemical composition of AISI H13 tool steel (wt.%)

C	Mn	Si	Cr	Mo	V	Ni	Fe
0.32–0.45	0.20–0.50	0.80–1.2	4.75–5.50	1.10–1.75	0.80–1.20	0–0.30	Bal.

in order to avoid rapid wear of the cutting tool at high cutting speeds.

All the milling tests were conducted in dry conditions and each trial was performed three times. The chatter mark on the machined surface of the workpiece can be used to evaluate the stability of the milling process. The machined surface was examined during the milling tests. It was found that there existed no obvious chatter mark on the machined surface at different cutting speeds. The cutting forces were measured using Kistler piezoelectric dynamometer (type 9257B) during the cutting process. Its measurement range and measurement accuracy were ±5 kN and 0.01 N, respectively. The dynamometer was installed on the machine table as shown in Fig. 1. The charge generated at the dynamometer was amplified by means of a multichannel charge amplifier. For the purpose of removing noise caused by the process variables, a low-pass filter was applied at the charge amplifier. The sampling frequency of data was set to be 10,000 Hz. The tool flank wear was examined with a digital microscope periodically. The microscope had a highest magnification of ×200. For each insert, the tool flank wear was measured three times and the average value was acquired. The tool life was recorded when the tool flank wear reached or increased over 0.3 mm. The tool life was recorded in terms of the number of cutting cycles. After the milling tests, the chip morphology and the worn tools were observed and analyzed using scanning electron microscopy (SEM; JSM-6510LV, Japan) and Keyence VHX-600E 3D digital microscope with a large depth of field. The highest magnification of JSM-6510LV was ×300,000, and it can provide high clarity of the specimen with a high resolution of 3.0 nm. The Keyence VHX-600E owned a highest magnification of ×5000.

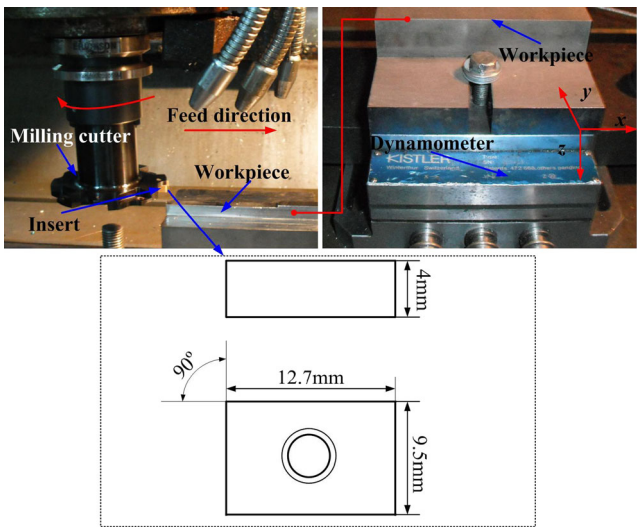

Fig. 1 Experimental setup

2.3 Finite element simulation

It was found from the cutting forces recorded in the milling process that cutting force in Z direction was much smaller than these in the X and Y directions. Moreover, the chip formation process is mainly caused by the interactions between the cutting tool and the workpiece in X and Y directions. Therefore, the milling process was modeled as a two-dimensional cutting process. Abaqus/Explicit software was used in the two-dimensional simulation of milling process in order to investigate quantities that were difficult to measure. Figure 2 shows the schematic of finite element simulation. The boundary conditions were set to be consistent with those in the milling experiments. Material properties of the workpiece and the cutting tool are listed in Table 2. The cutting tool was modeled as elastic and heat transfer body.

The use of a suitable material-constitutive model for the workpiece is important for simulating the cutting process successfully. The effects of stress, strain, strain rate, and temperature should be incorporated in the material model. The Johnson and Cook model has been widely applied in order to analyze the high-temperature, high strain-rate deformation behavior of steels. The Johnson and Cook constitutive equation was used in the present work. It can be expressed as:

$$\overline{\sigma} = \left[A + B\left(\overline{\varepsilon}\right)^{n}\right]\left[1 + C\ln\left(\frac{\dot{\overline{\varepsilon}}}{\dot{\overline{\varepsilon}}_0}\right)\right]\left[1-\left(\frac{T_{\mathrm{a}}-T_{\mathrm{room}}}{T_{\mathrm{melt}}-T_{\mathrm{room}}}\right)^{m}\right] \quad (1)$$

where $\overline{\varepsilon}$, $\dot{\overline{\varepsilon}}$, T_{a}, and $\overline{\sigma}$ are the shear strain, shear strain rate, absolute temperature, and shear stress, respectively. The material behaviors are mainly influenced by parameters such as the yield strength (A), the hardening modulus (B), the strain rate sensitivity (C), the strain hardening exponent (n), the thermal softening coefficient (m), the reference plastic strain ($\dot{\overline{\varepsilon}}_0$), the reference temperature (T_{room}), and the melting temperature (T_{melt}). These Johnson–Cook parameters was set to be A= 674.8 MPa, B=239.2 MPa, C=0.056, n=0.44, and m= 2.7 according to the work by Umer [16].

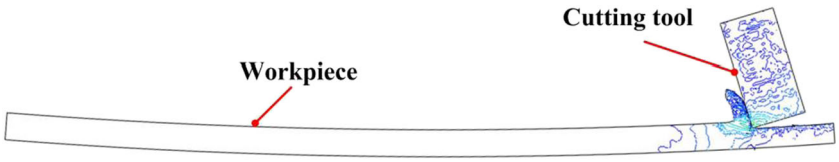

Fig. 2 Schematic of finite element simulation

The shear failure criterion was adopted in the present work in order to achieve separation of the chip from workpiece in the simulation process. For each element, the damage was calculated and can be expressed as:

$$\omega = \sum \frac{\Delta\varepsilon^{p}}{\varepsilon^{fp}} \tag{2}$$

where $\Delta\varepsilon^{p}$ is the cumulative equivalent plastic strain which is upgraded for each analysis increment, and ε^{fp} is the strain at which material failure happen. When the value of ω reached 1, element failure will occur. Simultaneously, the element, the element connectivity, the stress and the strain are deleted during the simulation process. The failure strain ε^{fp} can be given by:

$$\varepsilon^{fp} = \left[D_1 + D_2 \exp\left(D_3 \frac{\sigma_p}{\sigma_e}\right)\right]\left[1 + D_4 \ln\left(\frac{\dot{\varepsilon}^{p}}{\dot{\varepsilon}_0}\right)\right]\left[1 + D_5\left(\frac{T_a - T_{room}}{T_{melt} - T_{room}}\right)\right] \tag{3}$$

where D_1 to D_5 are damage parameters determined by experimental tests, σ_p/σ_e is the ratio of pressure stress to von Mises stress, and $\dot{\varepsilon}_0$ is the reference strain rate. The values of the damage parameters in Eq. (3) were determined by tensile and torsion tests of the workpiece material. These parameters were adopted from the work by Umer [16] and are listed in Table 3.

The tool-workpiece contact can be divided into sliding area and sticking area. According to the study by Atlati et al. [17], the contact behavior at the tool-workpiece interface can be defined as follow:

$$\tau_f = \begin{cases} \mu\sigma_n & \text{if} \quad \mu\sigma_n < \tau_{max} \\ \tau_{max} & \text{if} \quad \mu\sigma_n \geq \tau_{max} \end{cases} \tag{4}$$

where τ_f is the shear friction stress, σ_n is the normal friction stress, τ_{max} is the shear stress limit which can be considered as the initial plastic flow shear stress and μ is the friction coefficient. The friction coefficient μ was determined as the 0.41 based on the comparison of experimental and simulated cutting forces.

Table 2 Material properties of the workpiece and the cutting tool

Material properties	Workpiece	Cutting tool
Density (kg m^{-3})	7.72×10^{3}	14.5×10^{3}
Young's modulus (Pa)	2.12×10^{11}	6.24×10^{11}
Thermal expansion (K^{-1})	9.6×10^{-6}	5.3×10^{-6}
Heat capacity (J kg^{-1} K^{-1})	565	410
Thermal conductivity (W m^{-1} K^{-1})	28.5	81

3 Results and discussion

3.1 Chip formation

Comparisons of the chip obtained in milling tests and finite element simulation were conducted. Figure 3 shows the typical chip morphologies acquired at different cutting speeds in the experiments and simulation. It can be seen from Fig. 3 that the degree of serration of the simulated chip showed good consistency with that of the experimental chip. It was found that there existed no serrated chip at the cutting speed of 200 m/min. However, serrated chip arose at the other cutting speeds adopted in the present study. The serration of chip became more and more obvious as the cutting speed increased. It should be pointed out that some of the saw-tooth of the chip was separated at the cutting speed of 1550 m/min as shown in Fig. 3. Moreover, most of the saw-tooth was separated when the cutting speed was 2000 m/min.

Figure 4 shows the typical morphologies of the serrated chip that were about to be separated. It can be seen from regions A, B, C, and D denoted in Fig. 4 that the edges of the saw-tooth exhibited the characteristics of melted metal. It was inferred that high temperature arose in the area between the adjacent saw-tooth. Due to the high temperature, strength of this area degraded. When external loads were exerted on this area, crack appeared between the adjacent saw-tooth and the saw-tooth was separated.

Figure 5 shows the formation process of a separated saw-tooth which was obtained by means of finite element simulation. It can be observed from Fig. 5b that crack first arose in the shear band close to the cutting edge. It was found that the temperature of the area where the crack appeared was the highest in the shear band. It can be deduced that the high temperature had great effect on the initiation of the crack in the chip. Figure 5c indicated that the crack grew as the cutting tool moved forward and interacted with the workpiece. Then, another crack emerged in the shear band on the surface of the workpiece as shown in Fig. 5d. It can be seen from Fig. 5e, f

Table 3 Values of the damage parameters

D_1	D_2	D_3	D_4	D_5
−0.8	2.1	−0.5	0.0002	2.7

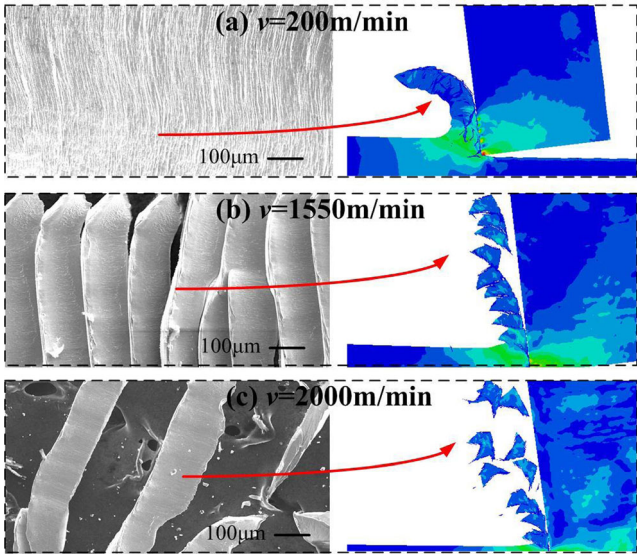

Fig. 3 Typical chip morphologies acquired at different cutting speeds in the milling tests and finite element simulation (v=200, 1550, and 2000 m/min)

that these two cracks propagated and finally met each other, resulting in the formation of an individual saw-tooth. It was found that the evolution of the cracks in the formation process of a separated saw-tooth was similar to that described by Guo and Yen [12]. These demonstrated the speculation that the high temperature in the area between the adjacent saw-tooth influenced the formation of the separated saw-tooth greatly.

The formation frequency f of the saw-tooth of the chip was calculated and analyzed. It was obtained using the following equation:

$$f = \frac{n_1 v}{60 l} \tag{5}$$

where n_1 is the number of saw-tooth per unit cutting distance, v is the cutting speed, l is the unit cutting distance. Figure 6 shows the evolution of formation frequency f with cutting speed v. It can be observed from Fig. 6 that as the cutting speed increased, the formation frequency of the saw-tooth kept increasing. However, the growth rate of the frequency decreased when the cutting speed increased.

Figure 7 shows the tool-chip contact areas at different cutting speeds. Figure 8 shows the development of tool-chip contact length L with cutting speed v. It can be observed from Figs. 7 and 8 that the tool-chip contact length exhibited a decreasing trend as the cutting speed increased from 200 to 2000 m/min. This can be attributed to the increased degree of

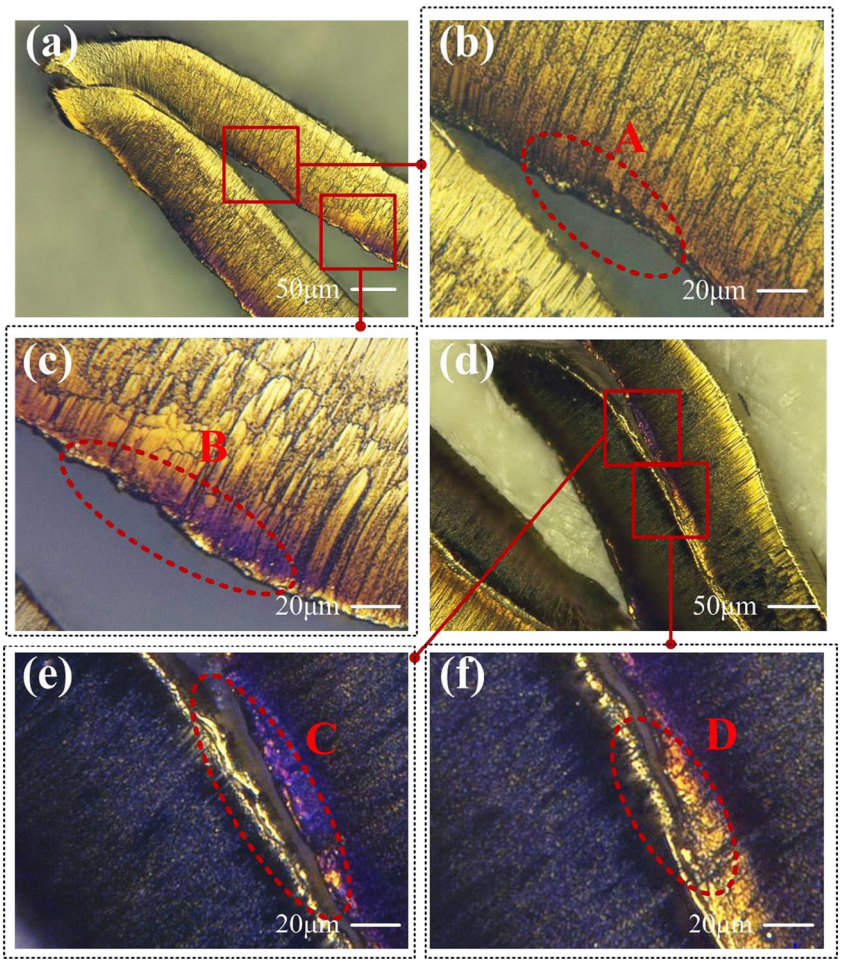

Fig. 4 Typical morphologies of the serrated chip that were about to be separated (v=2000 m/min)

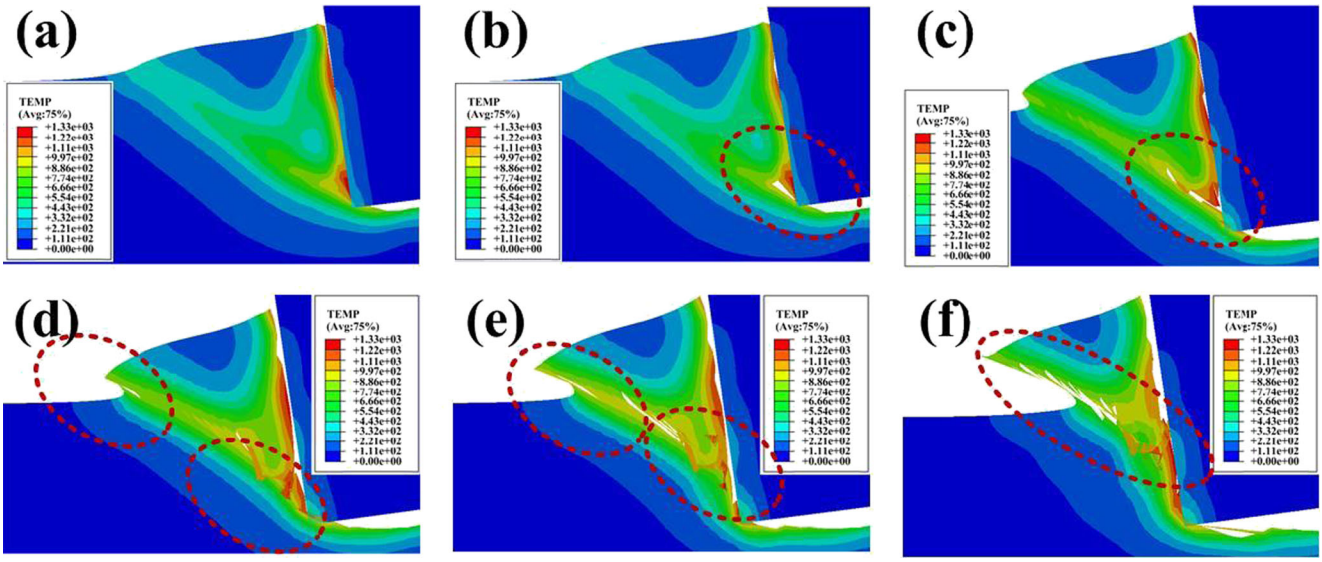

Fig. 5 Formation process of a separated saw-tooth (v=2000 m/min)

chip serration. It was found that substantial decrease of tool-chip contact length occurred as the cutting speed increased from 1550 to 2000 m/min. Taking the degree of chip serration at different cutting speeds into account, it can be deduced that the formation of separated saw-tooth chip led to great decrease of the tool-chip contact length.

3.2 Cutting forces and tool temperature

Figure 9 shows the comparisons of the average values of resultant cutting force F_{ra} (in X and Y directions) obtained in experimental tests and finite element simulation. It can be seen from Fig. 9 that the cutting force decreased as the cutting speed increased from 200 to 2000 m/min. Moreover, it can be found that the simulated cutting force was close to that obtained in the milling tests, which demonstrated the accuracy of the simulated results.

Figure 10 shows the typical evolution processes of resultant cutting forces F_r acquired at different cutting speeds.

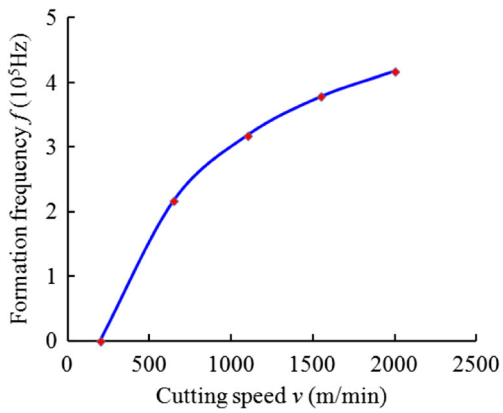

Fig. 6 Evolution of the formation frequency f of saw-tooth with cutting speed v (v=200, 650, 1100, 1550, and 2000 m/min)

There existed cutting period and non-cutting period in one cutting cycle in the milling process. In the present work, the time was set to be zero when half of the cutting period was finished. It can be observed from Fig. 10 that there existed no cyclical fluctuations of cutting force at the cutting speed of 200 m/min. However, fierce fluctuation of cutting force arose at cutting speeds of 1550 and 2000 m/min. The fluctuation frequency of cutting force was calculated and compared with that of saw-tooth formation. It was found that the fluctuation frequency of the cutting force at each cutting speed was consistent with that of the saw-tooth formation shown in Fig. 6. It can be deduced that the periodically changing cutting thickness resulted from the saw-tooth formation led to the cyclical fluctuation of the cutting force. The fluctuation of cutting force caused by chip segmentation was consistent with the analysis results obtained in previous studies [12, 17].

The amplitude A_F of the resultant cutting force was defined as:

$$A_F = \frac{F_P - F_v}{2} \tag{6}$$

where F_P and F_v denoted in Fig. 10 are the peak value and valley value of the resultant cutting force in a fluctuation cycle, respectively. The development of the amplitude A_F of resultant cutting force with cutting speed v is shown in Fig. 11. It can be seen from Fig. 11 that as the cutting speed increased, the amplitude of the cutting force exhibited an increasing trend. It was found that the amplitude of the cutting force obtained at cutting speed of 2000 m/min was 216 % of that acquired at 650 m/min. This was mainly caused by the increasing trend of the degree of chip serration with cutting speed. The higher degree of chip serration led to the substantial change of the cutting thickness during the saw-tooth formation process, which subsequently resulted in larger cutting force amplitude.

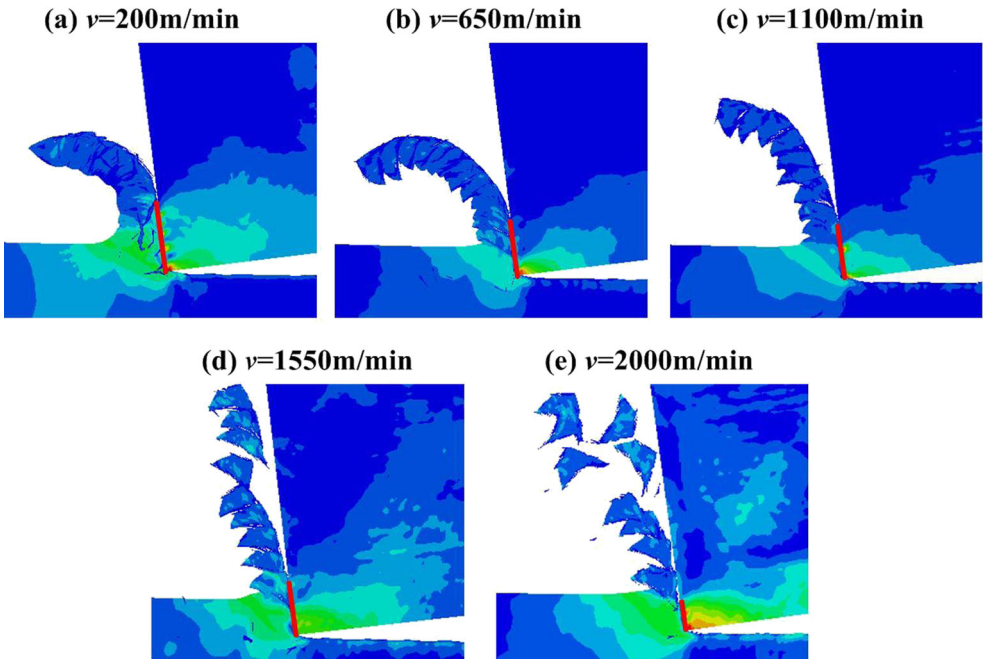

Fig. 7 Tool-chip contact areas at different cutting speeds (v=200, 650, 1100, 1550, and 2000 m/min)

The cutting edge temperature acquired in the simulation was acquired and analyzed in the present work. The development of the average value of tool temperature T_{ea} with cutting speed v is shown in Fig. 12. Figure 12 indicated that the cutting edge temperature kept increasing when the cutting speed increased. The evolving trend of the cutting edge temperature with cutting speed reflected the development of the temperature in the tool-chip contact area. Due to the thermal softening effects caused by higher temperature in such area, the cutting force decreased as the cutting speed increased as shown in Fig. 9.

The typical evolution processes of tool temperature T_e with cutting time t obtained at different cutting speeds are presented in Fig. 13. It can be observed from Fig. 13 that intense cyclical fluctuations of tool temperature arose at cutting speeds of 1550 and 2000 m/min. However, no cyclical fluctuation of tool temperature appeared at the cutting speed of 200 m/min. These phenomena were similar to those shown in Fig. 10. It was also found that the fluctuation frequency of the tool temperature at each adopted cutting speed was the same to that shown in Fig. 6. It seemed that the saw-tooth formation which resulted in periodically changing cutting thickness had substantial effects on the cyclical fluctuations of both cutting force and tool temperature.

The definition of the amplitude A_T of the tool temperature was similar to that of A_F. The amplitude A_T of the tool temperature was expressed as half of the gap between peak value T_P and valley value T_v shown in Fig. 13. Figure 14 shows the development of the amplitude A_T of tool temperature with cutting speed v. It can be observed from Fig. 14 that the amplitude A_T of the tool temperature showed an increasing trend as the cutting speed was raised. It can be found that the amplitude of tool temperature which arose at the cutting speed of

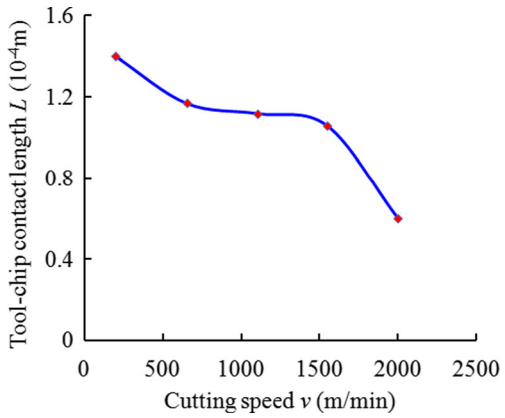

Fig. 8 Development of tool-chip contact length L with cutting speed v (v=200, 650, 1100, 1550, and 2000 m/min)

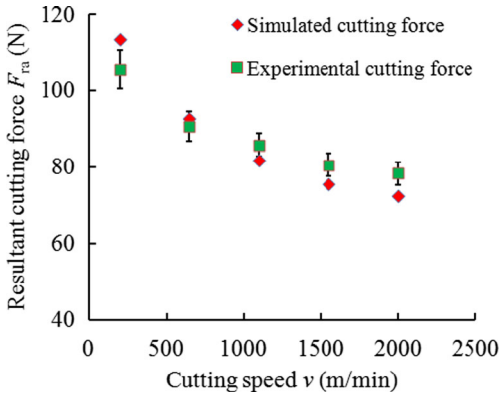

Fig. 9 Comparison of the average values of resultant cutting force F_{ra} obtained in experimental tests and finite element simulation (v=200, 650, 1100, 1550, and 2000 m/min)

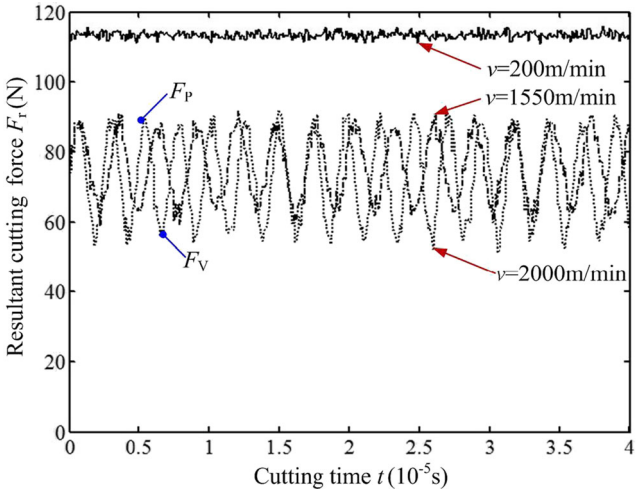

Fig. 10 Evolution of resultant cutting forces F_r with cutting time t in the cutting period (v=200, 1550, and 2000 m/min)

2000 m/min was 193 % of that which appeared at the cutting speed of 650 m/min. The increase of the degree of chip serration with cutting speed was the main reason why the tool temperature amplitude exhibited an increasing trend. Taking the evolution of the resultant cutting force amplitude A_F into consideration, it can be concluded that the substantial change of the cutting thickness caused by higher degree of chip serration had great effects on mechanical and thermal impact.

3.3 Tool stress and tool wear

In the present study, the maximum principal stress on the cutting edge was obtained and analyzed by means of finite element simulation. Figure 15 shows the development of the average value of tool stress S_{ea} with cutting speed v. It can be seen that the average tool stress increased with the increment of the cutting speed in spite of the decreasing trend of the cutting force shown in Fig. 9. This can be attributed to the larger value of tool temperature at higher cutting speed which has been presented in Fig. 12. It can be deduced that the tool

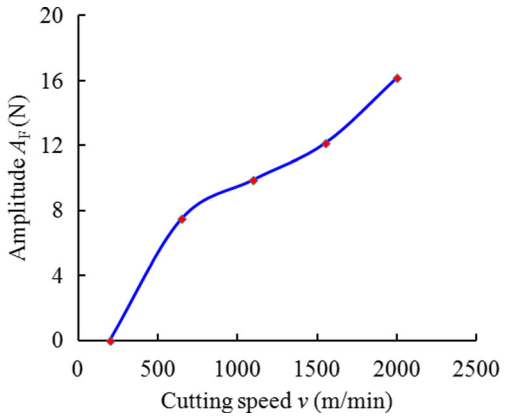

Fig. 11 Development of the amplitude A_F of resultant cutting force with cutting speed v (v=200, 650, 1100, 1550, and 2000 m/min)

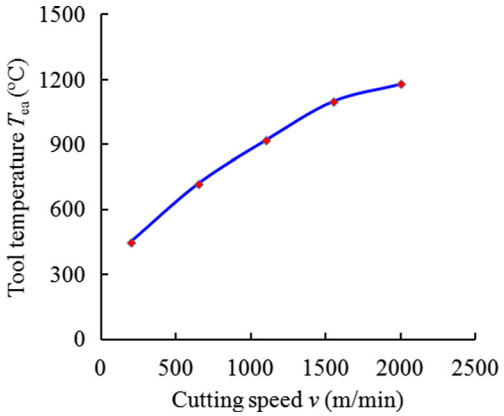

Fig. 12 Development of the average value of tool temperature T_{ea} with cutting speed v (v=200, 650, 1100, 1550, and 2000 m/min)

temperature has greater effect on the tool stress than the cutting force did at relatively high cutting speed.

The typical evolution processes of tool stress S_e with cutting time t are shown in Fig. 16. Taking the analysis of Figs. 10 and 13 into consideration, the cyclical fluctuations of tool stress which arose at cutting speeds of 1550 and 2000 m/min can be attributed to the combined effects of cyclical changing cutting force and tool temperature. It should be pointed out that as has been elaborated, the cyclical changing cutting force and tool temperature stemmed from the periodically changing cutting thickness induced by saw-tooth chip formation. Analysis of the fluctuation frequency of the tool stress at each cutting speed was performed. It was found that the fluctuation frequency of the tool stress was the same to that of the saw-tooth formation, cutting force, and tool temperature.

The amplitude A_S of the tool stress was investigated. It was defined to be half of the difference between peak value S_P and valley value S_v denoted in Fig. 16. Figure 17 presents the development of the amplitude A_S of tool stress with cutting

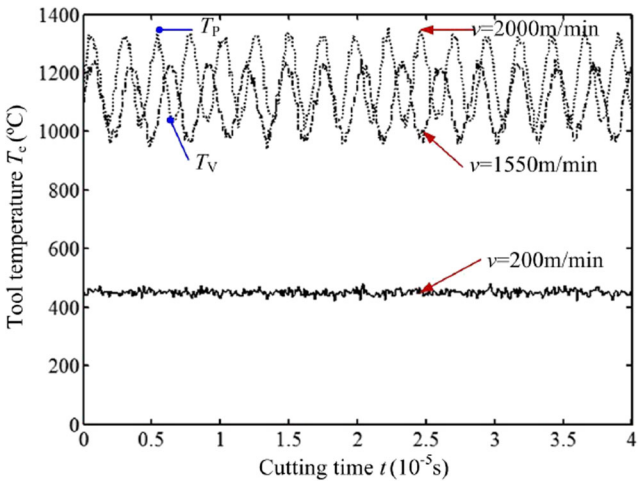

Fig. 13 Evolution of the tool temperature T_e with cutting time t (v=200, 1550, and 2000 m/min)

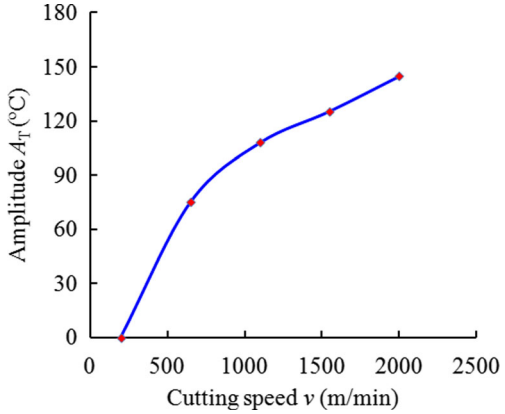

Fig. 14 Development of the amplitude A_T of tool temperature with cutting speed v (v=200, 650, 1100, 1550, and 2000 m/min)

speed v. Figure 17 indicates that when higher cutting speed was adopted, a larger value of the tool stress amplitude appeared. The larger value of the tool stress amplitude A_S which arose at higher cutting speed was mainly caused by the increasing trends of both A_F and A_T with cutting speed shown in Figs. 11 and 14.

In the present work, analysis of tool wear mechanisms focused on the cutting tools tested at relatively high cutting speeds (1550 and 2000 m/min). Figure 18 shows the typical morphologies of the cutting edge of the worn tools obtained at cutting speeds of 1550 and 2000 m/min. It can be observed from Fig. 18 that for the cutting tools tested at these cutting speeds, the main wear pattern of the cutting tool was flank wear and there seemed to be no obvious wear on the tool rake face. It has been shown in Fig. 8 that the tool-chip contact length was very small at the cutting speeds of 1550 and 2000 m/min. At the cutting speed of 2000 m/min, the emergence of the separated saw-tooth caused substantial decrease of the tool-chip contact length. These were the main reasons why no obvious wear appeared on the tool rake face. Previous investigation [3] also showed that there was no obvious wear on the tool rake face due to the short tool-chip contact length at relatively high cutting speed.

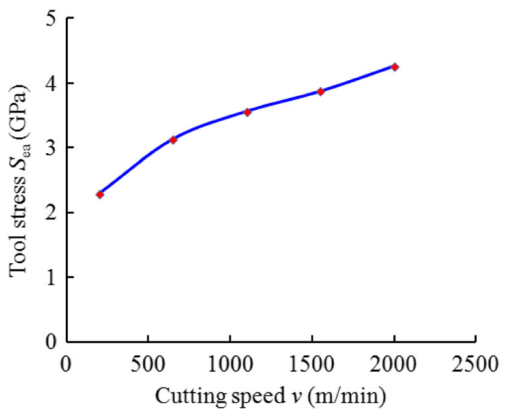

Fig. 15 Development of the average value of tool stress S_{ea} with cutting speed v (v=200, 650, 1100, 1550, and 2000 m/min)

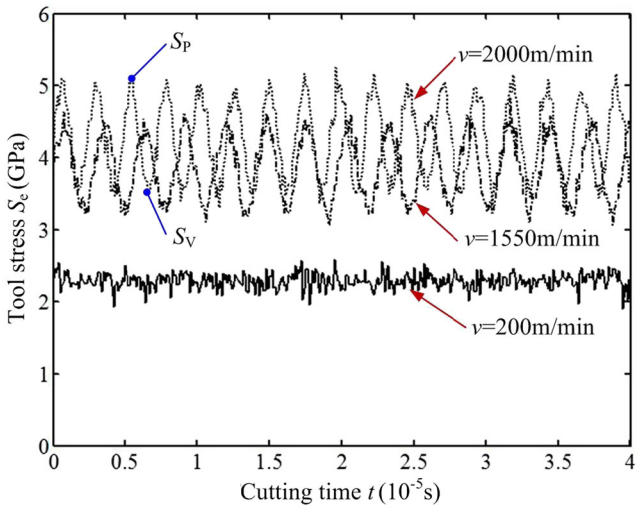

Fig. 16 Evolution of the tool stress S_e with cutting time t (v=200, 1550, and 2000 m/min)

The main difference between the worn tools obtained at cutting speeds of 1550 and 2000 m/min appeared at the cutting edge. It can be found from Fig. 18a, c that the main wear mechanisms of the cutting edge tested at the cutting speed of 1550 m/min was adhesion. Figure 18b, d shows that chipping arose on the cutting edge at the cutting speed of 2000 m/min. The average value and the amplitude of tool stress were higher at the cutting speed of 2000 m/min, indicating the combined effects of intenser thermal and mechanical impact in the cutting process. These led to the emergence of the chipping on the cutting edge at the cutting speed of 2000 m/min, which was not observed on the cutting edge when the tool was tested at 1550 m/min. It was also observed that there existed a crack close to the cutting edge for tools tested at cutting speeds of 1550 and 2000 m/min. This was mainly caused by the decay of the tool material property induced by high cutting temperature and relatively intense mechanical and thermal impact at higher cutting speed.

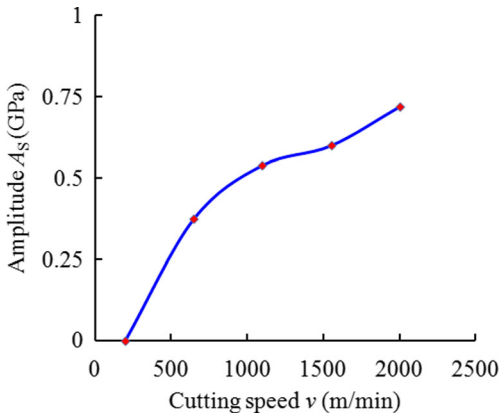

Fig. 17 Development of the amplitude A_S of tool stress with cutting speed v (v=200, 650, 1100, 1550, and 2000 m/min)

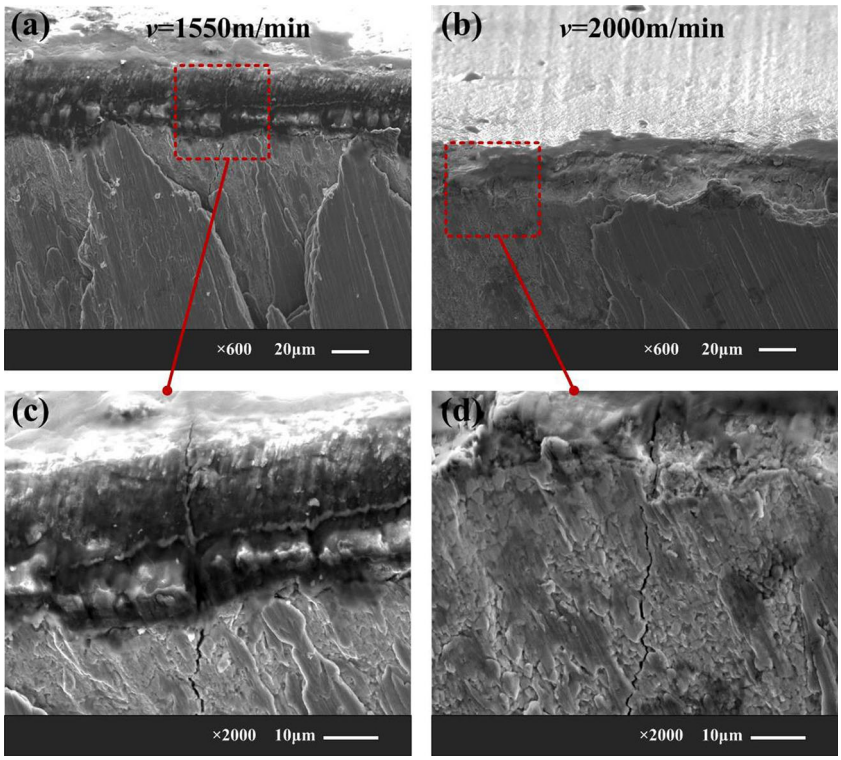

Fig. 18 Comparison of typical morphologies of the cutting edge of the worn tools obtained at cutting speeds of 1550 and 2000 m/min

4 Conclusions

In the present study, chip formation, cutting force, tool temperature, tool stress, and tool wear in high- and ultra-high-speed milling of AISI H13 hardened steel were investigated by means of experimental tests and finite element simulation. Effects of chip formation on mechanical load, thermal load, and wear of the tool cutting edge are analyzed. The following conclusions can be drawn from the present work:

- As the cutting speed increased, the serration of chip became more and more obvious. Most of the saw-tooth was separated at the cutting speed of 2000 m/min. The high temperature in the area between the adjacent saw-tooth had great effect on the formation of the separated saw-tooth. During the formation process of the separated saw-tooth, the initiation of the crack in the chip was influenced substantially by the high temperature in the shear band. When the cutting speed increased, the formation frequency of saw-tooth increased with decreasing growth rate. Due to the increased degree of chip serration, the tool-chip contact length showed a decreasing trend as the cutting speed increased. The formation of separated saw-tooth chip led to substantial decrease of the tool-chip contact length at cutting speed of 2000 m/min.
- The cutting force decreased with the increment of cutting speed. In contrast, the tool temperature exhibited an opposite evolving trend. The fluctuation frequency of cutting force and tool temperature at each cutting speed was consistent with that of the saw-tooth formation. The saw-tooth formation which led to periodically changing cutting thickness had substantial effects on the cyclical fluctuations of both cutting force and tool temperature. As the cutting speed increased, the amplitude of both the cutting force and tool temperature exhibited an increasing trend. As the cutting speed increased from 650 to 2000 m/min, the amplitude of cutting force and tool temperature grew 116 and 93 %, respectively. The higher degree of chip serration at higher cutting speed led to the substantial change of the cutting thickness, resulting in greater mechanical and thermal impact.
- When the cutting speed was relatively high, the tool temperature has greater effect on the tool stress than cutting force did. Due to the combined effects of cyclical changing cutting force and tool temperature, cyclical fluctuations of tool stress arose at cutting speeds of 1550 and 2000 m/min. It was found that the fluctuation frequency of the tool stress was the same to that of saw-tooth formation, cutting force, and tool temperature. The increasing trends of both cutting force A_F and tool temperature amplitude A_T with cutting speed resulted in the larger value of the tool stress amplitude A_S which arose at higher cutting speed. Because of the small tool-chip contact length at the cutting speeds of 1550 and 2000 m/min, there was no obvious wear on the tool rake face. The higher average value and the amplitude of tool stress at cutting speed of 2000 m/min led to the emergence of

chipping on the cutting edge, which was not observed on the cutting edge when the tool was tested at 1550 m/min.

Acknowledgments This research is supported by the National Natural Science Foundation of China (51475148), the Foundation of Henan Educational Committee (15A460005), the Fundamental Research Funds for the Universities of Henan Province (NSFRF140123), and the Doctor Foundation from Henan Polytechnic University (B2014-032).

References

1. Wang CY, Xie YX, Zheng LJ, Qin Z, Tang DW, Song YX (2014) Research on the chip formation mechanism during the high-speed milling of hardened steel. Int J Mach Tools Manuf 79:31–48
2. Su GS, Liu ZQ (2012) Wear characteristics of nano TiAlN-coated carbide tools in ultra-high speed machining of AerMet100. Wear 289:124–131
3. Cui X, Zhao J (2014) Cutting performance of coated carbide tools in high-speed face milling of AISI H13 hardened steel. Int J Adv Manuf Technol 71(9-12):1811–1824
4. Salomon CJ (1931) Process for machining metals of similar acting materials when being worked by cutting tools. German patent, Number 523594
5. Cui X, Zhao J, Tian X (2012) Tool wear in high-speed face milling of AISI H13 steel. Proc Inst Mech Eng B J Eng Manuf 226(10): 1684–1693
6. Liu ZQ, Su GS (2012) Characteristics of chip evolution with elevating cutting speed from low to very high. Int J Mach Tools Manuf 54–55:82–85
7. Su GS (2011) Evolution and mechanisms of saw-tooth chip formation in high-speed machining. Ph.D. thesis, Shandong University, Jinan
8. Molinari A, Musquar C, Sutter G (2002) Adiabatic shear banding in high speed machining of Ti–6Al–4V: experiments and modeling. Int J Plast 18(4):443–459
9. Ye GG, Xue SF, Ma W, Jiang MQ, Ling Z, Tong XH, Dai LH (2012) Cutting AISI 1045 steel at very high speeds. Int J Mach Tools Manuf 56:1–9
10. Shaw MC, Vyas A (1993) Chip formation in the machining of hardened steel. CIRP Ann 42(1):29–33
11. Vyas A, Shaw MC (1999) Mechanics of saw-tooth chip formation in metal cutting. J Manuf Sci Eng Trans ASME 121(2):163–172
12. Guo YB, Yen DW (2004) A FEM study on mechanisms of discontinuous chip formation in hard machining. J Mater Process Technol 155–156:1350–1356
13. Ding TC, Zhang S, Wang YW, Zhu XL (2010) Empirical models and optimal cutting parameters for cutting forces and surface roughness in hard milling of AISI H13 steel. Int J Adv Manuf Technol 51: 45–55
14. Cui X, Zhao J, Jia C, Zhou Y (2012) Surface roughness and chip formation in high-speed face milling AISI H13 steel. Int J Adv Manuf Technol 61:1–13
15. Zhang S, Li JF, Wang YW (2012) Tool life and cutting forces in end milling Inconel 718 under dry and minimum quantity cooling lubrication cutting conditions. J Clean Prod 32:81–87
16. Umer U (2012) High speed turning of H-13 tool steel using ceramics and PCBN. J Mater Eng Perform 21(9):1857–1861
17. Atlati S, Haddag B, Nouari M, Zenasni M (2011) Analysis of a new segmentation intensity ratio "SIR" to characterize the chip segmentation process in machining ductile metals. Int J Mach Tools Manuf 51(9):687–700